

Article

Optimization and Tunability of 2D Graphene and 1D Carbon Nanotube Electrocatalysts Structure for PEM Fuel Cells

Emeline Remy ¹, Yohann. R. J. Thomas ¹ , Laure Guetaz ², Frédéric Fouada-Onana ¹,
Pierre-André Jacques ¹ and Marie Heitzmann ^{1,*} 

¹ CEA, LITEN, DEHT, LCP, Univ. Grenoble Alpes, 17 rue des Martyrs, 38000 Grenoble, France; emeline.remy@gmail.com (E.R.); yoh.tho@gmail.com (Y.R.J.T.); frederic.fouada-onana@cea.fr (F.F.-O.); pierre-andre.jacques@cea.fr (P.-A.J.)

² CEA, LITEN, DTNM, L2N, Univ. Grenoble Alpes, 17 rue des Martyrs, 38000 Grenoble, France; laure.guetaz@cea.fr

* Correspondence: marie.heitzmann@cea.fr; Tel.: +33-478-380-4402

Received: 3 August 2018; Accepted: 25 August 2018; Published: 5 September 2018



Abstract: In this work, N-doped Multi-Walled Carbon Nanotubes (MWCNTs) and Few Graphene Layers (FGLs) have been functionalized with platinum nanoparticles using two methods starting with hexachloroplatinic acid as precursor: (i) ethylene glycol (EG) reduction and (ii) impregnation followed by reduction in hydrogen atmosphere. Morphological scanning transmission electron microscopy (STEM) analyses showed a homogenous dispersion of metal particles with narrow-size distribution onto both carbon supports (Pt/C loadings between 30 wt % and 40 wt %). Electrocatalytic properties of the as-synthesized catalysts toward the Oxygen Reduction Reaction (ORR) was evaluated in aqueous electrolyte using a three electrodes electrochemical cell by cyclic voltammetry (CV) in rotating disk electrode (RDE). It is shown that a mixture of Pt supported on MWCNT and FGLs allows to enhance both the electrochemical surface area and the activity of the catalyst layer. Ageing tests performed on that optimized active layer showed higher stability than conventional Pt/C.

Keywords: PEMFC; MWCNTs (Multi Wall Carbon Nanotube); graphene; nanostructured catalyst support; durability/stability

1. Introduction

The development of energy storage and conversion technologies has been intensified in recent years. Today, Polymer Electrolyte Membrane Fuel Cells (PEMFC), which convert the energy of a fuel such as hydrogen into electricity and heat has been recognized as an environmentally friendly technology of choice for transport application because of its low operation temperature, high energy efficiency and high power density [1].

The use of platinum based electrocatalysts is mandatory on both anode and cathode sides to significantly accelerate the electrochemical reactions which drive the PEMFC. The cathode especially where the oxygen reduction reaction (ORR) occurred request a non-negligible amount of Pt at the cathode (around 0.4 mg_{Pt}/cm² of electrode) which makes the technology dependent of that scarce metal [2]. A significant challenge for the commercial viability of PEMFCs resides is the decrease of Pt loading. For that, both the activity and stability of the used catalysts need to be enhanced [3,4]. Different ways such as the nanostructuring of catalyst particles or stabilization of the support are proposed to tackle those issues [5,6].

Another way to reduce the Pt loading is to make most of the Pt atoms that are present active for the ORR. Therefore the active layer should be optimized to find the best trade-off between mass transport,

interfacial reactions at electrochemically active sites, proton transport and electronic conduction. It has been recognized that platinum nanoparticles supported on carbon allow to fit those requirements. The carbon support plays a critical role in terms of active layer performances and stability [7–12].

Nowadays, carbon black (especially Vulcan XC72) is the most commonly used as nanoparticle support because of its large specific surface area, high availability, high electrical conductivity, pore structure and low cost [12]. However, it suffers from thermochemical instability and from corrosion caused by electrochemical oxidation under fuel cell operating condition (high potential, temperature around 80 °C, presence of water, low pH) [13,14]. Indeed, carbon black is known to undergo electrochemical oxidation to surface oxides and eventually to CO₂ at the cathode side. Moreover, the corrosion rate of carbon catalyst support is accelerated in the presence of Pt-containing catalysts [15–17] and under specific operating events of the PEMFC such as start and stop [18]. As carbon is corroded away, noble metal nanoparticles (NPs) will be either lost from the electrode or aggregated to larger particles and structural change of the AL are observed such as AL thinning. Those mechanisms have been well presented in a recent review and reference within [19].

Even if some groups propose alternative support to carbon such as doped metal oxide, they faced some issue regarding electronic conductivity and stability [20], therefore, most of the effort have been directed to identify and synthesize alternative carbon materials as catalyst supports for PEMFCs. One strategy to decrease carbon support corrosion is to use carbon with high extent of graphitization, which is supposed to decrease defect sites on the carbon structure, where carbon oxidation starts [21,22]. Among the different forms of carbon, carbon nanotubes and more recently graphene have attracted tremendous interest over many conventional catalyst support materials for various energy applications [23,24]. Indeed, the combination of their high surface area, high conductivity and high chemical stability makes these 1D and 2D materials promising candidates for cathode catalyst support in PEMFCs [25]. However, high graphitic content of carbon can be a brake for particle nucleation and dispersion. Therefore, in our work we have use N-doped CNT has support to facilitate Pt NPs deposition [26,27].

In this paper, we investigated the properties of 2D FGLs/1D MWCNTs Pt catalysts for electrocatalysis of oxygen reduction. By comparing the electrochemical properties of these hybrid materials with a reference Pt/C (46 wt %-Pt Tanaka Kikinzoku Kogyo, Japan reference TEC10V50E) catalyst using carbon blacks as support, it is found that this hybrid material demonstrated an enhancement of electro-catalyst performances in RDE tests. Moreover, accelerated stress tests (ASTs) demonstrated that the use of this FGLs and MWCNTs support can be promising in effectively reducing the loss of electrochemical surface area (ECSA).

2. Results

2.1. STEM, UV and TGA Analyses

Scanning transmission electron microscopy (STEM) images showing the morphology of Pt NPs on the three carbon supports are presented in Figure 1. The particle size distribution, obtained by a statistical study from 300 Pt NPs, for all samples is reported in Table 1. For carbon nanotubes support (Figure 1a,b), a large number of Pt NPs are distributed on tube walls quite uniformly and do not aggregate to form larger clusters, indicating a strong interaction between CNTs support and particles. This can be attributed to the use of N-doped MWCNTs as support. From these images it can also be noticed that the Pt NPs are on the outside of the multi walled carbon nanotubes. The average Pt particle size was calculated to be $d_{\text{TEM}} = 3.5$ nm (Table 1). Note that these values are in the range of particle size reported in the literature [28,29].

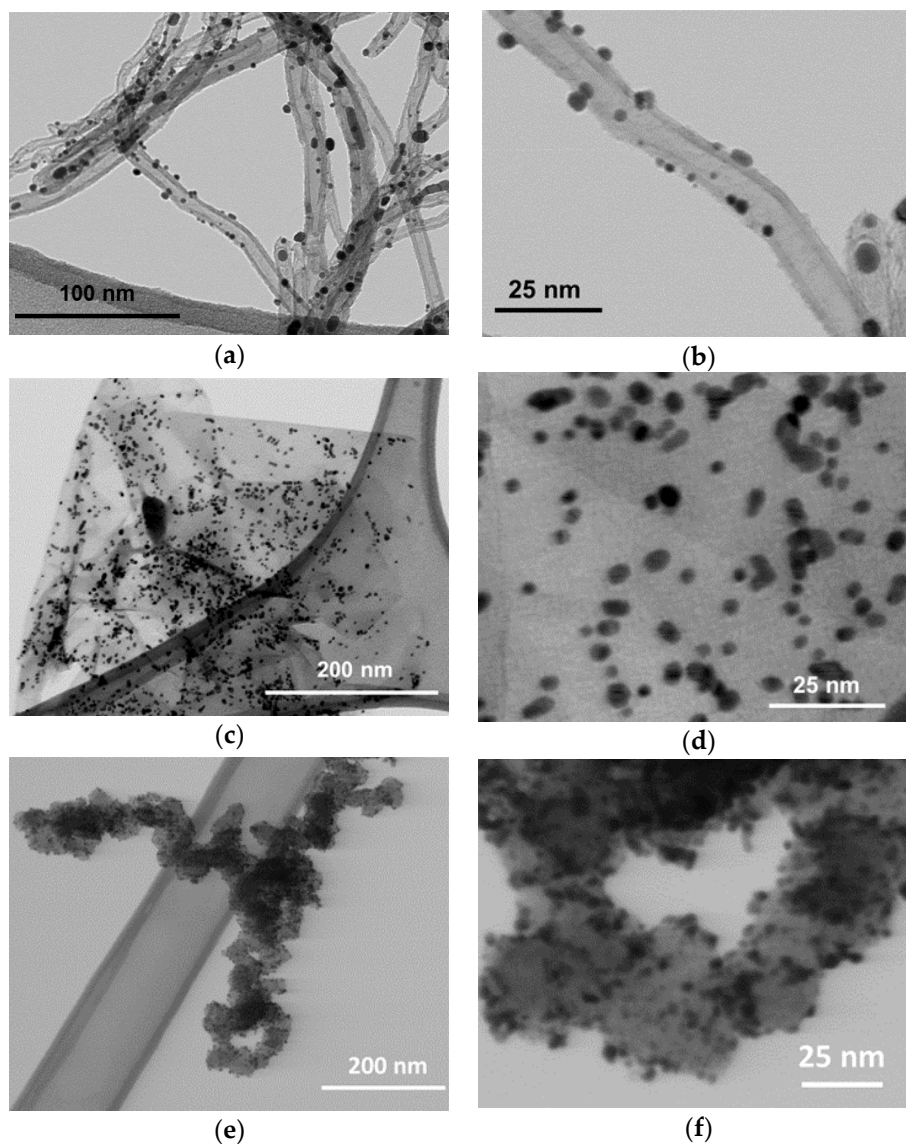


Figure 1. STEM images of Pt catalyst (a,b) deposit on MWCNTs by thermal treatment, (c,d) Pt deposit on FGLs by chemical reduction, (e,f) Pt on carbon blacks TEC10V50E.

Table 1. Particle size distribution for electrocatalysts Pt/C, Pt/MWCNTs and Pt/FGLs determined by statistical STEM study.

Electrocatalyst	Mean Particle Diameter TEM (nm)
Pt/C	3.4
Pt/MWCNTs	3.5
Pt/FGLs	4.3

Concerning the FGLs support (Figure 1c,d), transparent and well-formed 2D planar sheets are observed [30]. This Pt/FGLs catalyst exhibits a wider distribution with particle sizes between 1 and 7.5 nm, with a mean size of 3.6 nm (Figure 1f). These STEM studies concluded that Pt NPs are fairly uniform with the optimum particle size on the two carbon supports. These features are both desired for good catalyst performance and durability since it is well known that the activity of a catalyst depends considerably on the size of the Pt particles and their dispersion over the support [12,31].

The metal loading of the Pt/FGLs (31 wt %) and Pt/MWCNTs (37 wt %) determined by UV spectroscopy were close to the targeted value (40 wt %). The high Pt loading for MWCNTs support is mainly attributable to the high chemical attractiveness of N-doped MWCNTs, the presence of heteroatom making easier the NPs nucleation than on FGL [32].

The thermogravimetric analysis (TGA) profiles measured in flowing air for all samples are shown in Figure 2. The degradation temperatures for Pt/FGLs, Pt/MWCNTs and Pt/C were 620, 510 and 400 °C, respectively (Figure 2 full line). This result suggests that the thermal stability or the resistance to oxidation of Pt/FGLs is higher than Pt/MWCNTs and Pt/C catalysts due to increasing ratio of graphitization. We can also note that the Pt NPs accelerate the support degradation, in fact it is known that platinum nanoparticles have catalytic effects on carbon decomposition. Moreover, this sample weight residual confirms the previous UV quantification.

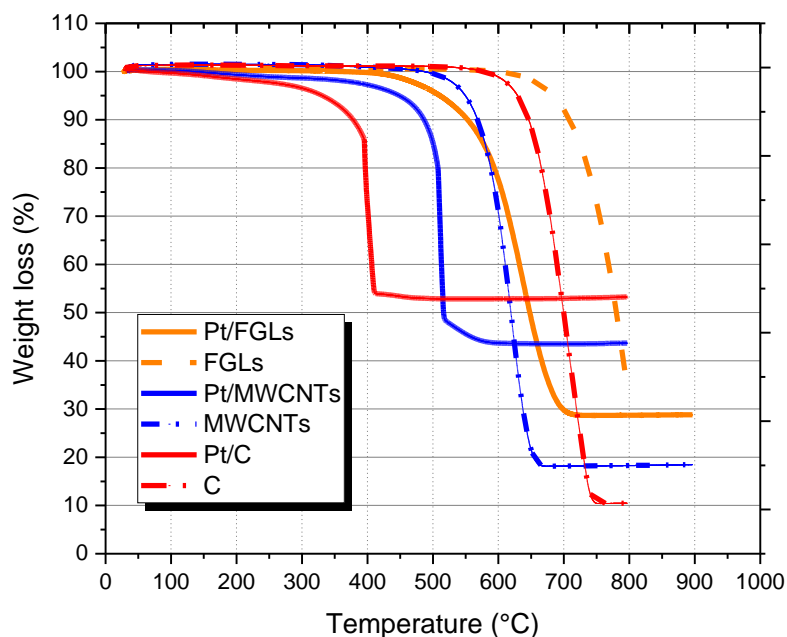


Figure 2. TGA profiles of the samples, in dotted line before Pt deposition and in full line after Pt deposition.

2.2. RDE

The electrochemical characteristics i.e., ECSA and ORR activity of synthesized catalysts evaluated using a rotating disk electrode in a 0.5M H₂SO₄ aqueous solution are shown in Figure 3. The CV curves in the voltage range from 0.04 V to 1.2 V at a scan rate of 5 mVs⁻¹ for the Pt/C, Pt/FGLs, Pt/MWCNTs and a mechanical mixture of these two catalysts with five different weight ratios, denoted as Pt/(FGLs + MWCNTs), are shown in Figure 3a. Figure 3b shows the calculated current density deduced from the polarization curves for ORR and the electrochemically active surface area (ECSA) of each catalyst and the comparison with Pt/C. The RDE voltamograms at a rotation rate of 900 rpm were used to evaluate and compare the ORR kinetic current densities at 0.9 V vs. RHE of all catalysts.

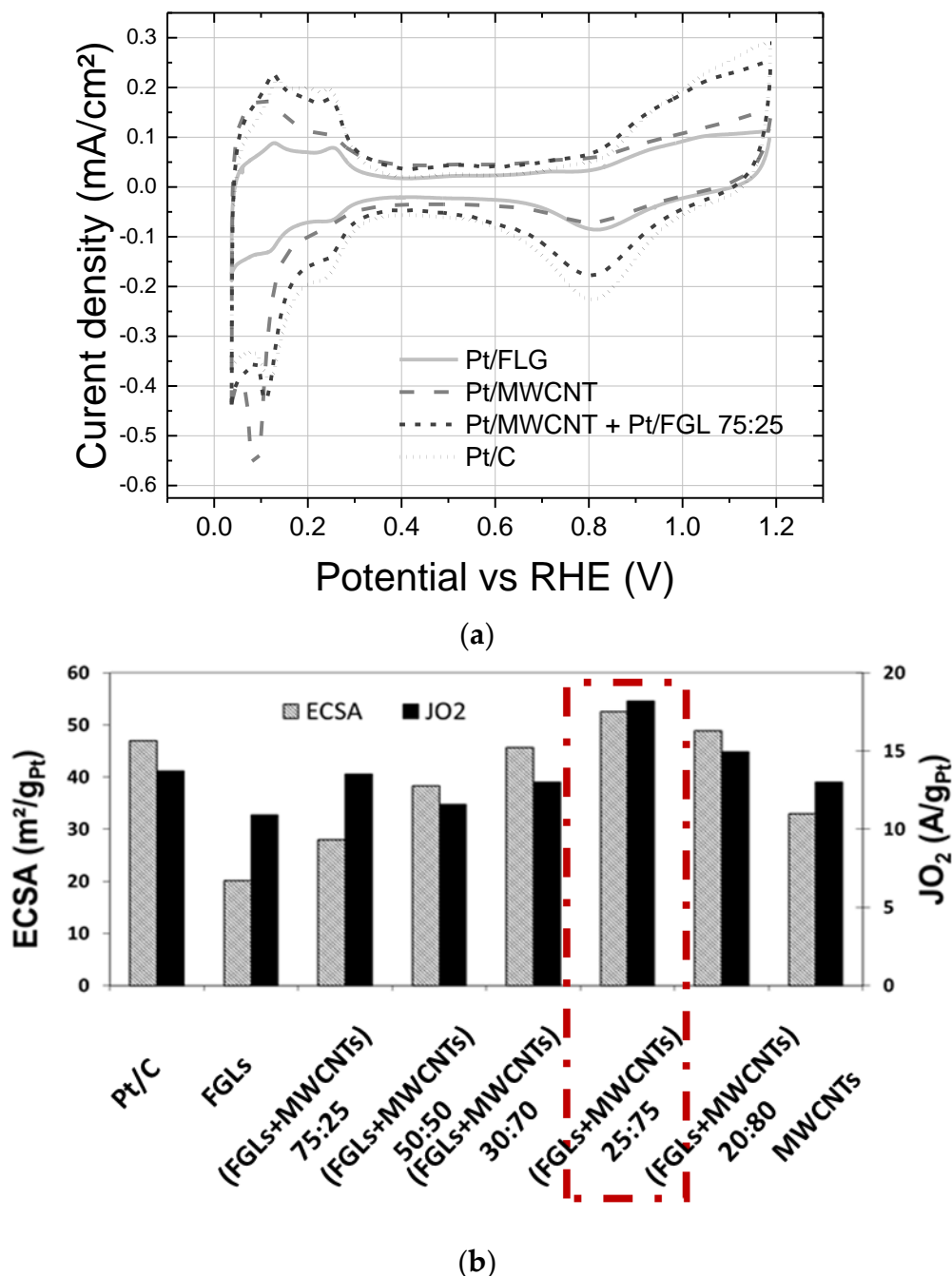


Figure 3. (a) Comparison of the cyclic voltammograms of the catalysts in 0.5 M H₂SO₄, 5 mV·s⁻¹ and (b) the calculated ECSA and current density for the as-prepared catalysts compared with commercial catalyst.

The CVs of all catalysts exhibit typical electro-adsorption/desorption of hydrogen at Pt sites. The response from the Pt(110) and Pt(100) surfaces for hydrogen adsorption and desorption is visible for these catalysts. The flat wave around 0.2 V in the hydrogen under-potential deposition (HUPD) is typical of small Pt NPs [33]. The ECSA, which is a measure of the number of electrochemically active sites per gram of the catalyst, is calculated from the mean value of the coulombic charge exchanged during the electro-desorption of hydrogen using 210 $\mu\text{C}/\text{cm}^2\text{Pt}$ after correcting for the electric double layer contribution.

The different tested mixtures let appear a volcano graph with an optimum for the mixture 25:75 for which the highest calculated performances of 53 m²/gPt and 18 A/gPt are obtained, outperforming

thus the commercial Pt catalyst ($47 \text{ m}^2/\text{gPt}$ and 14 A/gPt). It can also be noticed that this hybrid FGLs + MWCNTs material achieved largely higher performances than 100% of Pt/MWCNTs ($32 \text{ m}^2/\text{gPt}$ and 13 A/gPt) or 100% of Pt/FGLs showing the lowest performances ($19 \text{ m}^2/\text{gPt}$ and 12 A/gPt).

2.3. Ageing Test

We conducted ageing tests on this hybrid material using 3 different accelerated stressed tests based on (a) CV from 0.3 to 1.18 V Vs RHE with a scan rate of $20 \text{ mV}\cdot\text{s}^{-1}$ (b) CV from 0.6 to 1.0 V Vs RHE with a scan rate of $50 \text{ mV}\cdot\text{s}^{-1}$ and (c) CV from 1.0 to 1.5 V Vs RHE with a scan rate of $500 \text{ mV}\cdot\text{s}^{-1}$ in order to test support stability at high potential (from 1 to 1.5 V Vs RHE) and catalyst stability (AST from 0.6 to 1V vs RHE). The ECSA was regularly measured during the cycles of the AST and plotted in Figure 4. The 3 tests showed higher ECSA stability for the composite (Pt/MWCNT-Pt/FLG). At the end of the first AST, 48% of the initial ECSA of the composite (Pt/MWCNT-Pt/FLG) is remained while the reference Pt/C retain only 30% of its ECSA showing thus a better tolerance toward degradation of our designed catalyst layer. Then AST design for catalyst dissolution (AST (b)) and support corrosion (AST (c)) showed a higher ECSA stability for our designed active layer. AST for catalyst dissolution allowed us to do more cycles (30k cycles) because of its less drastic conditions the the AST test for carbon support corrosion (5k cycles). The use of structured carbon as support might be less sensitive toward oxidation and thus avoiding particles coarsening while the N-doped NTC might stabilized the NPs.

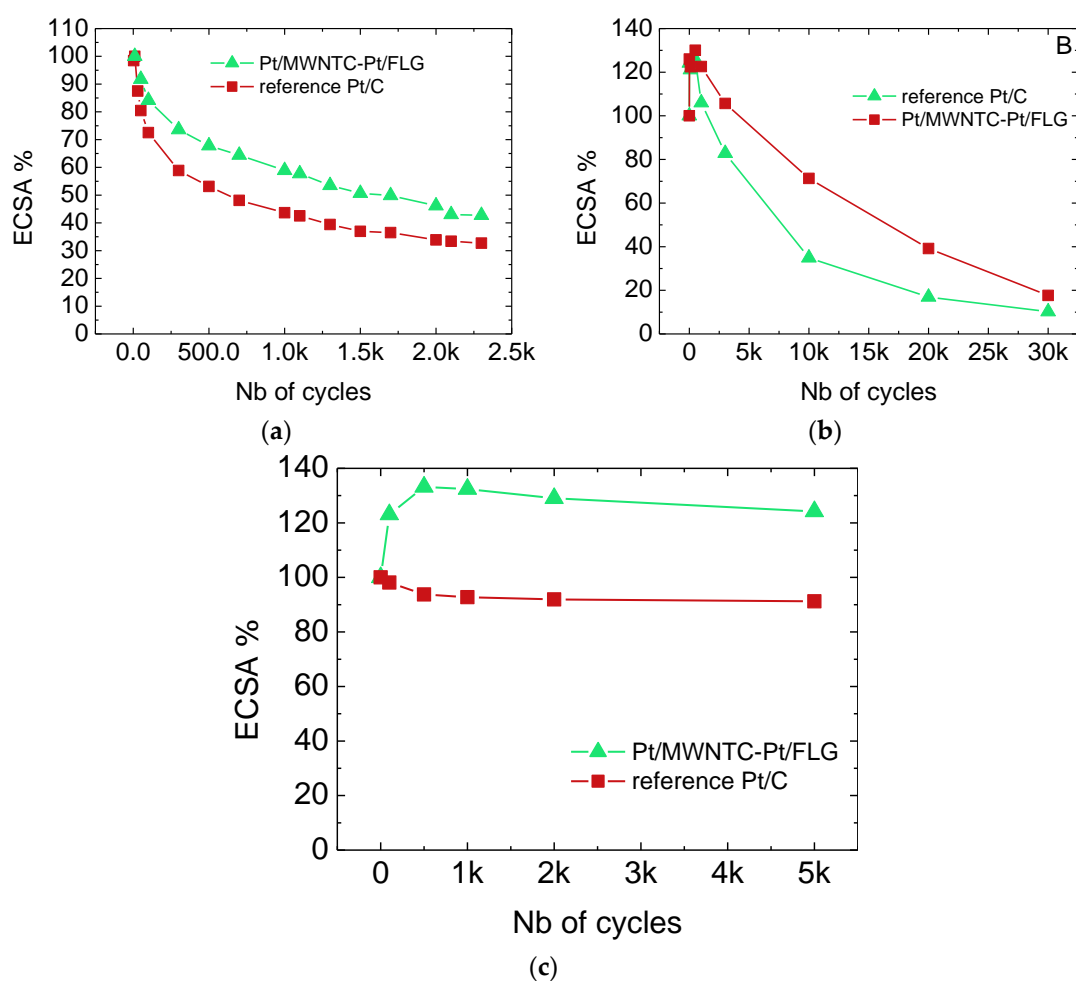


Figure 4. (a) CV from 0.3 to 1.18 V Vs RHE with a scan rate of $20 \text{ mV}\cdot\text{s}^{-1}$ (b) CV from 0.6 to 1.0 V Vs RHE with a scan rate of $50 \text{ mV}\cdot\text{s}^{-1}$ and (c) CV from 1.0 to 1.5 V Vs RHE with a scan rate of $500 \text{ mV}\cdot\text{s}^{-1}$.

3. Discussion

As demonstrated by Gasteiger [34], and assuming spherical particles, a theoretical value of active surface, denoted as STEM can be calculated from the following equations:

$$S_v = 6 \left(\frac{1000}{\rho_{Pt} \bar{d}} \right)$$

$$\bar{d}_{v/a} = \left(\frac{\sum_{i=1}^n d_i^3}{\sum_{i=1}^n d_i^2} \right)$$

where d is the mean platinum particle radius diameter calculated thanks to the catalyst size distribution analysis from TEM images, d the diameter of each individual particles and ρ_{Pt} equal to 21.45 g/cm³. For the mixture of 75:25 we also considered the same ratio for the whole distribution particle size to calculate the mean particle diameter of the mixture and the STEM. The Pt utilization percentage for each catalyst is deduced from the ratio (ECSA/STEM) \times 100 and compared in Table 2.

Table 2. Comparison of the particle diameter (TEM), calculated particle surface (STEM), ECSA (RDE) and the Pt utilization percentage of the employed electrocatalysts.

Electrocatalyst	Mean Particle Diameter TEM (nm)	Surface TEM (m ² /g _{Pt})	Real Electrochemical Surface (m ² /g _{Pt})	Pt Utilization %
Pt/C	3.4	82	47	57
Pt/MWCNTs	3.5	80	32	40
Pt/FGLs	4.3	65	19	29
Pt/(FGLs + MWCNTs) 75:25	4.0	70	53	76

From these results, it can be noticed that the value of Pt utilization obtained for Pt/C sample (50%) is lower when compared with literature. In particular Ferreira et al. [34] obtained for commercial Pt/C that roughly 70% of the apparent area of platinum particles is electrochemically active. We believe that this is probably due to the high loading of the RDE WE (100 μg_{Pt}·cm⁻²) used in our study. A thick layer of catalyst is deposited on the WE surface resulting in mass transport limitations.

From these results, it appears that the ECSA measured on CV represents only 29% and 40% for FGLs and MWCNTs catalysts respectively of the real surface area of the catalyst as determined by TEM. This can be due to the non-utilization of the contact surface between platinum and carbon in the electrochemical reaction, to the aggregation of crystallites or more probably to a bad accessibility of the H⁺ to the Pt NPs due to agglomeration of MWCNTs or FGLs by π-stacking which prevents a good contact between Pt NPs and electrolyte. For Pt/(FGLs + MWCNTs) it appears that the value is 76% which is about twice the ratio of FGLs and slightly higher compared with the Pt/C sample.

This result seems to suggest that the homogeneous mechanical mixing of high surface area 2D-FGLs and high conductive 1D-MWCNTs results in 3D hybrid composite, which exhibits very good electrochemical performances for ORR. In our opinion, it results first from the optimization of the active layer porosity. In particular, the addition of MWCNTs in an optimal ratio in the FGL matrix may disrupt the preferred horizontal stacking of graphene sheets and makes them randomly distributed in the catalytical layer. This configuration induces a porous network structure which then facilitate the simultaneous access between Pt NPs and reactant. The available triple-phase boundary is increased and the mass transport limitation reduced, as illustrated in Figure 4. The second reason is the improvement of the active layer electrical conductivity by hybridization of these two carbon nanostructures. More precisely, MWCNTs act as conducting bridges between the FGLs while FGLs act as spacer between CNTs increasing thus the number of available catalyst particles for ORR. This conclusion comforts the trend reported in literature, showing that the reactant diffusion in graphene containing layer can be improved by using porous graphene [35] or composite [36].

In conclusion, we synthesized a new catalyst for PEMFC based on the functionalization of graphene and N-doped CNT by Pt nanoparticles, an appropriate mixture of those these two catalysts (1D Pt/MWCNT and 2D Pt/GFLs) allowed us to design a 3D active layer based with comparable performance and better corrosion resistance properties and higher stability toward reference Pt/C.

4. Materials and Methods

4.1. Catalyst Preparation

Commercial FGLs and N-doped MWCNTs were provided by Angstrom and Nanocyl societies, respectively. Pt catalysts supported on FGLs are prepared by ethylene glycol reduction [37]. 200 mg of FGLs in 180 mL of deionized (DI)-water (Milli-Q water 18.2 M Ω cm, Direct-Q 3, Millipore, Burlington, MA, USA) were sonicated for 15 min to obtain a homogenous dispersion. At the same time, 350 mg of H₂PtCl₆.6H₂O (ref 520896-5G from Sigma-Aldrich, St. Louis, MO, USA, purity >99.9%) were solubilized in 20 mL of DI water. This solution was then added dropwise into the dispersion and sonicated for another 15 min. This mixture was added to 250 mL of EG (from Sigma-Aldrich, purity >99.5%) in a 500 mL flask. The reduction reaction was then performed at 110 °C for 12 h with constant stirring. The Pt NPs/FGLs catalysts were finally separated by vacuum filtration and washed several times with DI water and acetone. The resulting product was dried at 95 °C for 48 h. These sample is denoted as Pt/FGLs.

Pt catalysts based on N-doped MWCNTs are prepared by thermal treatment under reductive atmosphere [38]. Indeed, it is well known that since the pristine surface of CNTs is relatively inert, it is difficult to have a high dispersion of Pt NPs with controlled catalyst loading on the surface of support. It is believed that these surface functional groups act as metal-anchoring sites to facilitated metal nuclei formation and electrocatalyst deposition [30,31]. Furthermore, the insertion of N atom in the graphitic structure of the MWCNT gives a C–N bond close to a carbo nitride structure which is known to be more tolerant towards corrosion than oxygenated carbon [32,33]. In a typical synthesis, 600 mg of N-doped MWCNTs were dispersed in 500 mL of Di-water by ultrasonicated mixing for 1 h. At the same time, 1 g of H₂PtCl₆.6H₂O was dissolved in 100 mL of DI-water. This solution was then added slowly to the catalyst solution and sonicated for 1 h. Impregnation step was carried out for 12 h under constant and magnetic stirring at room temperature. Finally, the powder is separated from the solvent with a vacuum rotary evaporator and grounded in an agate mortar. The resulting powder was heated in a tube furnace at 300 °C under H₂/Ar (10:90) flow for 3 h. This sample is denoted as Pt/MWCNTs.

The targeted value of Pt loading for this two catalyst is 40 wt %.

Mixtures of Pt on FGLs and Pt on MWCNTs were also prepared. This hybrid material, denoted as Pt/(FGLs + MWCNTs), was made by a mechanical mixture of these two catalysts with five different weight ratios of FGLs + MWCNTs: 20/80; 25/75; 30/70; 50/50; 75/25. In fact, after weighing the two powders at the desired ratio (Pt/FGL and Pt/MWCNT), the powders are quickly mixed mechanically in the same container and, after adding solvent, the ink is homogenized in an ultrasonic bath.

4.2. Electrochemical Methods

The electrochemical properties of the prepared samples were investigated by a conventional three-electrode system in 0.5 M H₂SO₄ solution at room temperature. Working electrodes were prepared by mixing the catalyst with Nafion[®] dispersion (type D-520 from Dupont Fluoroproducts, 5% Nafion[®] dissolved in aliphatic alcohols), isopropanol and water. After homogenization in an ultrasonic bath or with an ultrasonic probe to avoid particles agglomeration, about 40 μ L of this suspension was deposited onto a glassy carbon disk (area 0.2475 cm²). After solvent evaporation under air at 80 °C, a thin layer of catalyst ink remained on the working electrode surface and the Pt loading on the RDE was calculated as 100 μ g_{Pt}·cm⁻². The counter electrode was a Pt wire and a saturated mercury sulfate electrode (MSE) (Bioanalytical Systems Inc., RE-2C) was employed as a reference; all potentials are referred to the Reference Hydrogen Electrode (RHE) potential (i.e., +0.687 V versus

MSE). Before each measurement the electrolyte solution was saturated by pure nitrogen for 30 min in order to expel oxygen. Three cyclic voltammograms (CV) were carried out at room temperature between 0.04 and 1.2 V vs. RHE at $20 \text{ mV}\cdot\text{s}^{-1}$ and $5 \text{ mV}\cdot\text{s}^{-1}$. The electrochemical active area of Pt was determined from the integrated charge under the hydrogen adsorption peaks in the second cycle after correction of the capacitive effect attributed to the electrochemical double layer. The polarization curves of the ORR were carried out in H_2SO_4 solution saturated with O_2 applying linear potential sweep from 0.04 V to 1.2 V at a rotating rate of 900 rpm and a scan rate of $5 \text{ mV}\cdot\text{s}^{-1}$.

The catalyst has been aged under accelerated stress tests (AST) which has been described more precisely in the discussion part.

4.3. Electron Microscopy

Electron microscopy analyses were performed on a scanning electron microscope Hitachi 5500 operating in STEM mode using a voltage of 30 kV. For sample preparation, each catalyst powder was dispersed in ethanol using a low power sonication bath and a drop of the liquid solution was deposited on a lacey carbon TEM copper grid. The nanoparticle size histogram was built using a statistical analysis (300 NPs) by means of software ImageJ (National Institutes of Health, Bethesda, MD, USA).

4.4. UV Quantification

To quantify the actual amount of metal loaded on the carbon support, UV spectroscopy analysis measurements were carried out by using a Shimadzu 1800 UV spectrometer. The catalysts powder are initially heat treated in a ceramic oven at $600 \text{ }^\circ\text{C}$ for 15 h so that all the components other than Pt are oxidized and vented out of the furnace. The remaining Pt catalyst powder is chemically treated to convert it to the Pt^{4+} ionic form, which is needed to perform the UV measurements. The treatment consists in the dilution of the Pt catalyst powder in a solution of 25 vol % HNO_3 and 75 vol % HCl (Aqua Regia). The solution is completely evaporated at $100 \text{ }^\circ\text{C}$ into a dedicated glass system. This step is repeated twice with concentrated HCl (12 M). The obtained dry catalyst is finally diluted in HCl (1 M) where the Pt^{4+} ions are stable. The obtained solution is analyzed to determine the catalyst concentration. A calibration of the UV spectrometer was made before each measurement by using reference samples.

4.5. TGA

The thermogravimetric analysis of the samples was measured with a TGA 92-12 Setaram analyzer using a $10 \text{ }^\circ\text{C}\cdot\text{min}^{-1}$ heating rate, until reaching $900 \text{ }^\circ\text{C}$, under air flow ($30 \text{ mL}\cdot\text{min}^{-1}$). Under these conditions, carbonaceous species are burnt off and only the metal-based particles remain at $900 \text{ }^\circ\text{C}$.

Author Contributions: E.R. and Y.R.J.T. performed the experiments, E.R, Y.R.J.T. and F.F.-O. analyzed the data, L.G. performed STEM analysis. E.R., P.-A.J. and M.H. wrote and revised the paper.

Funding: The research leading to these results has received funding from the European Union's Seventh Framework Programme (FP7/2007-2013) for Fuel Cell and Hydrogen Joint Technology Initiative under Grant No. 325239 (NanoCAT) and from the Flagship program internally funded by CEA.

Acknowledgments: The authors thank the European Union's Seventh Framework program (Grant No. 325239 project NANOCAT) for the funding and Nanocyl for kind supply of nanostructure carbon support.

Conflicts of Interest: The authors declare no conflicts of interest.

References

1. Chen, S.; Wei, Z. Recent Advances of Electrocatalyst, Catalyst Utilization and Water Management in Polymer Electrolyte Membrane Fuel Cells. Available online: <http://www.ingentaconnect.com/content/asp/sam/2015/00000007/00000010/art00011> (accessed on 16 July 2018).

2. Gasteiger, H.A.; Marković, N.M. Just a Dream—Or Future Reality? *Science* **2009**, *324*, 48–49. [[CrossRef](#)] [[PubMed](#)]
3. Shao, Y.; Yin, G.; Gao, Y. Understanding and approaches for the durability issues of Pt-based catalysts for PEM fuel cell. *J. Power Sources* **2007**, *171*, 558–566. [[CrossRef](#)]
4. Uchimura, M.; Sugawara, S.; Suzuki, Y.; Zhang, J.; Kocha, S.S. Electrocatalyst Durability under Simulated Automotive Drive Cycles. *ECS Trans.* **2008**, *16*, 225–234. [[CrossRef](#)]
5. Lv, H.; Li, D.; Strmcnik, D.; Paulikas, A.P.; Markovic, N.M.; Stamenkovic, V.R. Recent advances in the design of tailored nanomaterials for efficient oxygen reduction reaction. *Nano Energy* **2016**, *29*, 149–165. [[CrossRef](#)]
6. Strasser, P.; Kühn, S. Dealloyed Pt-based core-shell oxygen reduction electrocatalysts. *Nano Energy* **2016**, *29*, 166–177. [[CrossRef](#)]
7. Gasteiger, H.A.; Baker, D.R.; Carter, R.N.; Gu, W.; Liu, Y.; Wagner, F.T.; Yu, P.T. *Hydrogen and Fuel Cells: Fundamentals, Technologies and Applications*; Contributions to the 18th World Hydrogen Energy Conference 2010, Essen; Stolten, D., Ed.; Wiley-VCH: Weinheim, Germany, 2011; ISBN 978-3-527-32711-9.
8. Sharma, S.; Pollet, B.G. Support materials for PEMFC and DMFC electrocatalysts—A review. *J. Power Sources* **2012**, *208*, 96–119. [[CrossRef](#)]
9. Speder, J.; Zana, A.; Spanos, I.; Kirkensgaard, J.J.K.; Mortensen, K.; Hanzlik, M.; Arenz, M. Comparative degradation study of carbon supported proton exchange membrane fuel cell electrocatalysts—The influence of the platinum to carbon ratio on the degradation rate. *J. Power Sources* **2014**, *261*, 14–22. [[CrossRef](#)]
10. Stevens, D.A.; Hicks, M.T.; Haugen, G.M.; Dahn, J.R. Ex Situ and In Situ Stability Studies of PEMFC Catalysts Effect of Carbon Type and Humidification on Degradation of the Carbon. *J. Electrochem. Soc.* **2005**, *152*, A2309–A2315. [[CrossRef](#)]
11. Wu, J.; Yuan, X.Z.; Martin, J.J.; Wang, H.; Zhang, J.; Shen, J.; Wu, S.; Merida, W. A review of PEM fuel cell durability: Degradation mechanisms and mitigation strategies. *J. Power Sources* **2008**, *184*, 104–119. [[CrossRef](#)]
12. Yaldagard, M.; Jahanshahi, M.; Seghatoleslami, N. Carbonaceous Nanostructured Support Materials for Low Temperature Fuel Cell Electrocatalysts—A Review. *World J. Nano Sci. Eng.* **2013**, *3*, 121–153. [[CrossRef](#)]
13. Antolini, E. Carbon supports for low-temperature fuel cell catalysts. *Appl. Catal. B Environ.* **2009**, *88*, 1–24. [[CrossRef](#)]
14. Kangasniemi, K.H.; Condit, D.A.; Jarvi, T.D. Characterization of Vulcan Electrochemically Oxidized under Simulated PEM Fuel Cell Conditions. *J. Electrochem. Soc.* **2004**, *151*, E125–E132. [[CrossRef](#)]
15. Mukundan, R.; James, G.; Ayotte, D.; Davey, J.R.; Langlois, D.; Spornjak, D.; Torrace, D.; Balasubramanian, S.; Weber, A.Z.; More, K.L.; et al. Accelerated Testing of Carbon Corrosion and Membrane Degradation in PEM Fuel Cells. *ECS Trans.* **2013**, *50*, 1003–1010. [[CrossRef](#)]
16. Roen, L.M.; Paik, C.H.; Jarvi, T.D. Electrocatalytic Corrosion of Carbon Support in PEMFC Cathodes. *Electrochem. Solid-State Lett.* **2004**, *7*, A19–A22. [[CrossRef](#)]
17. Speder, J.; Zana, A.; Spanos, I.; Kirkensgaard, J.J.K.; Mortensen, K.; Arenz, M. On the influence of the Pt to carbon ratio on the degradation of high surface area carbon supported PEM fuel cell electrocatalysts. *Electrochem. Commun.* **2013**, *34*, 153–156. [[CrossRef](#)]
18. Durst, J.; Lamibrac, A.; Charlot, F.; Dillet, J.; Castanheira, L.F.; Maranzana, G.; Dubau, L.; Maillard, F.; Chatenet, M.; Lottin, O. Degradation heterogeneities induced by repetitive start/stop events in proton exchange membrane fuel cell: Inlet vs. outlet and channel vs. land. *Appl. Catal. B Environ.* **2013**, *138–139*, 416–426. [[CrossRef](#)]
19. Dubau, L.; Castanheira, L.; Maillard, F.; Chatenet, M.; Lottin, O.; Maranzana, G.; Dillet, J.; Lamibrac, A.; Perrin, J.-C.; Moukheiber, E.; et al. A review of PEM fuel cell durability: Materials degradation, local heterogeneities of aging and possible mitigation strategies. *Wiley Interdiscip. Rev. Energy Environ.* **2014**, *3*, 540–560. [[CrossRef](#)]
20. Cognard, G.; Ozouf, G.; Beauger, C.; Dubau, L.; López-Haro, M.; Chatenet, M.; Maillard, F. Insights into the stability of Pt nanoparticles supported on antimony-doped tin oxide in different potential ranges. *Électrochim. Acta* **2017**, *245*, 993–1004. [[CrossRef](#)]
21. Bom, D.; Andrews, R.; Jacques, D.; Anthony, J.; Chen, B.; Meier, M.S.; Selegue, J.P. Thermogravimetric Analysis of the Oxidation of Multiwalled Carbon Nanotubes: Evidence for the Role of Defect Sites in Carbon Nanotube Chemistry. *Nano Lett.* **2002**, *2*, 615–619. Available online: <https://pubs.acs.org/doi/abs/10.1021/nl020297u> (accessed on 17 July 2018). [[CrossRef](#)]

22. Wang, X.; Li, W.; Chen, Z.; Waje, M.; Yan, Y. Durability investigation of carbon nanotube as catalyst support for proton exchange membrane fuel cell. *J. Power Sources* **2006**, *158*, 154–159. [CrossRef]
23. Cheng, Y.; Lu, S.; Zhang, H.; Varanasi, C.V.; Liu, J. Synergistic Effects from Graphene and Carbon Nanotubes Enable Flexible and Robust Electrodes for High-Performance Supercapacitors. *Nano Lett.* **2012**, *12*, 4206–4211. Available online: <https://pubs.acs.org/doi/abs/10.1021/nl301804c> (accessed on 17 July 2018). [CrossRef] [PubMed]
24. Zhou, X.; Qiao, J.; Yang, L.; Zhang, J. A Review of Graphene-Based Nanostructural Materials for Both Catalyst Supports and Metal-Free Catalysts in PEM Fuel Cell Oxygen Reduction Reactions. *Adv. Energy Mater.* **2014**, *4*, 1301523. [CrossRef]
25. Fu, K.; Wang, Y.; Qian, Y.; Mao, L.; Jin, J.; Yang, S.; Li, G. Synergistic Effect of Nitrogen Doping and MWCNT Intercalation for the Graphene Hybrid Support for Pt Nanoparticles with Exemplary Oxygen Reduction Reaction Performance. *Materials* **2018**, *11*, 642. [CrossRef] [PubMed]
26. Chen, Y.; Wang, J.; Liu, H.; Banis, M.N.; Li, R.; Sun, X.; Sham, T.-K.; Ye, S.; Knights, S. Nitrogen Doping Effects on Carbon Nanotubes and the Origin of the Enhanced Electrocatalytic Activity of Supported Pt for Proton-Exchange Membrane Fuel Cells. *J. Phys. Chem. C* **2011**, *115*, 3769–3776. [CrossRef]
27. Higgins, D.C.; Meza, D.; Chen, Z. Nitrogen-Doped Carbon Nanotubes as Platinum Catalyst Supports for Oxygen Reduction Reaction in Proton Exchange Membrane Fuel Cells. *J. Phys. Chem. C* **2010**, *114*, 21982–21988. [CrossRef]
28. Liu, Z.; Gan, L.M.; Hong, L.; Chen, W.; Lee, J.Y. Carbon-supported Pt nanoparticles as catalysts for proton exchange membrane fuel cells. *J. Power Sources* **2005**, *139*, 73–78. [CrossRef]
29. Saha, M.S.; Neburchilov, V.; Ghosh, D.; Zhang, J. Nanomaterials-supported Pt catalysts for proton exchange membrane fuel cells. *Wiley Interdiscip. Rev. Energy Environ.* **2012**, *2*, 31–51. [CrossRef]
30. Wang, Y.; Shao, Y.; Matson, D.W.; Li, J.; Lin, Y. Nitrogen-Doped Graphene and Its Application in Electrochemical Biosensing. *ACS Nano* **2010**, *4*, 1790–1798. [CrossRef] [PubMed]
31. Nores-Pondal, F.J.; Vilella, I.M.J.; Troiani, H.; Granada, M.; de Miguel, S.R.; Scelza, O.A.; Corti, H.R. Catalytic activity vs. size correlation in platinum catalysts of PEM fuel cells prepared on carbon black by different methods. *Int. J. Hydrog. Energy* **2009**, *34*, 8193–8203. [CrossRef]
32. Fang, B.; Kim, M.-S.; Kim, J.H.; Song, M.Y.; Wang, Y.-J.; Wang, H.; Wilkinson, D.P.; Yu, J.-S. High Pt loading on functionalized multiwall carbon nanotubes as a highly efficient cathode electrocatalyst for proton exchange membrane fuel cells. *J. Mater. Chem.* **2011**, *21*, 8066–8073. [CrossRef]
33. Will, F.G. Hydrogen Adsorption on Platinum Single Crystal Electrodes I. Isotherms and Heats of Adsorption. *J. Electrochem. Soc.* **1965**, *112*, 451–455. [CrossRef]
34. Ferreira, P.J.; Shao-Horn, Y.; Morgan, D.; Makharia, R.; Kocha, S.; Gasteiger, H.A. Instability of Pt/C Electrocatalysts in Proton Exchange Membrane Fuel Cells A Mechanistic Investigation. *J. Electrochem. Soc.* **2005**, *152*, A2256–A2271. [CrossRef]
35. Cheng, K.; He, D.; Peng, T.; Lv, H.; Pan, M.; Mu, S. Porous graphene supported Pt catalysts for proton exchange membrane fuel cells. *Électrochim. Acta* **2014**, *132*, 356–363. [CrossRef]
36. Higgins, D.C.; Hassan, F.M.; Seo, M.H.; Choi, J.Y.; Hoque, M.A.; Lee, D.U.; Chen, Z. Shape-controlled octahedral cobalt disulfide nanoparticles supported on nitrogen and sulfur-doped graphene/carbon nanotube composites for oxygen reduction in acidic electrolyte. *J. Mater. Chem. A* **2015**, *3*, 6340–6350. [CrossRef]
37. Grinou, A.; Yun, Y.S.; Cho, S.Y.; Park, H.H.; Jin, H.-J. Dispersion of Pt Nanoparticle-Doped Reduced Graphene Oxide Using Aniline as a Stabilizer. *Materials* **2012**, *5*, 2927–2936. [CrossRef]
38. Choi, S.M.; Seo, M.H.; Kim, H.J.; Kim, W.B. Synthesis and characterization of graphene-supported metal nanoparticles by impregnation method with heat treatment in H₂ atmosphere. *Synth. Met.* **2011**, *161*, 2405–2411. [CrossRef]

